Research Square

Preprints are preliminary reports that have not undergone peer review.
They should not be considered conclusive, used to inform clinical practice,
or referenced by the media as validated information.

Highly selective small molecule Kv1.3 inhibitors bind to a cryptic pocket and stabilize the channel in a C-type inactive conformation

Joachim Vilstrup

JoachimVilstrup@outlook.com

Muna Therapeutics

Matilde Trabuco

LeadXpro AG https://orcid.org/0000-0001-9234-8685

Elmeri Jokinen

Aurlide https://orcid.org/0000-0003-2352-6550

Gavin Whitlock

Sandexis Ltd

Lars Christian Rønn

Muna Therapeutics

Marianne Pedersen

University of Copenhagen

Mathieu Botte

leadXpro AG

Florian Delbart

LeadXpro

Christoph Sager

Idorsia Pharmaceuticals Ltd. https://orcid.org/0000-0002-1481-9514

Olli Pentikäinen

Aurlide https://orcid.org/0000-0001-7188-4016

Michael Hennig

LeadXpro AG https://orcid.org/0000-0002-1839-2351

Jakob Busch-Petersen

Muna Therapeutics

Kim Andersen

Muna Therapeutics

Article

Keywords:

Posted Date: June 4th, 2026

DOI: https://doi.org/10.21203/rs.3.rs-9859541/v1

License: This work is licensed under a Creative Commons Attribution 4.0 International License.
Read Full License

Additional Declarations:
Yes there is potential Competing Interest. J.V., K.A., M.T.P., L.C.R. and J.B.P. are current or previous employees of Muna Therapeutics which owns patents related to the inhibitors described in this study. The remaining authors declare no competing interests.

Tables are available in the Supplementary Files section.

Highly selective small molecule Kv1.3 inhibitors bind to a cryptic pocket and stabilize the channel in a C-type inactive conformation

Joachim Vilstrup[1]*, Matilde Trabuco[2], Elmeri M. Jokinen[3], Gavin Whitlock[4], Lars Christian Rønn[1], Marianne Terndrup Pedersen[1], Mathieu Botte[2], Florian Delbart[2], Christoph P. Sager[2], Olli T. Pentikäinen[3], Michael Hennig[2], Jakob Busch-Petersen[1] and Kim Andersen[1]

Affiliations:
[1]Muna Therapeutics, Nordre Fasanvej 215, DK-2000 Frederiksberg, Denmark.
[2]LeadXpro, Park Innovaare, Parkstrasse 1, CH-5234 Villigen, Switzerland
[3]Aurlide, Lemminkäisenkatu 14-18A, FI-20520 Turku, Finland
[4]Sandexis Ltd, Innovation House, Discovery Park, CT13 9FF, Sandwich, United Kingdoms

* Corresponding author contact information: vilstrup@munatherapeutics.com

Abstract

The voltage-gated potassium ion channel Kv1.3 is an attractive therapeutic target due to its central role in effector memory T cell activation and autoimmune disease. Achieving subtype-selective inhibition remains challenging due to the high sequence conservation across the Kv1 family and the lack of structural insight into binding for selective small molecule inhibitors. Here, using a ligand-based virtual screening approach seeded from an existing dichlorophenol scaffold, we identify a novel indole-based chemotype as a highly selective small molecule inhibitor of human Kv1.3. Through a combination of site-directed mutagenesis and cryoEM, we map the binding site and elucidate the inhibitory mechanism of both chemotypes. We show that dichlorophenol and indole inhibitors bind to a cryptic pocket in the P-loop adjacent to the selectivity filter, with four ligands occupying this site per Kv1.3 tetramer. Inhibitor binding induces an expansion of the selectivity filter, disrupts key hydrogen bonds, and stabilizes a channel conformation resembling the C-type inactivated state. This inhibitory mechanism is distinct from a pore block and accesses a site previously restricted to peptide-based inhibitors. This study provides the first atomic-level view of small molecule engagement to Kv1.3 and expanding the mechanistic repertoire of voltage-gated ion channel inhibition. Together, our findings enable future comparison of state-dependent inhibition and downstream effector function while establishing a structural framework for the rational development of selective small molecule voltage-gated ion channel therapeutics.

Introduction

The voltage-gated potassium (Kv) ion channel 1.3 plays a central role in T cells by maintaining the membrane potential required for sustained calcium ion influx during T cell receptor activation, thereby driving downstream effector functions[1,2]. Kv1.3 is thus a potential therapeutic target in T cell–mediated autoimmune diseases[3–5] reviewed in ref.[6].

However, other Kv channels as well as other Kv1 subtypes govern repolarization in cardiomyocytes and neurons[7], making selective inhibition essential to minimize off-target effects and to isolate the disease-relevant functions of Kv1.3 specifically.

Voltage-gated potassium ion channels are key regulators of membrane excitability controlling potassium ion efflux and electrical signaling across diverse cell types[8]. The Shaker-related Kv1 family consists of eight subtypes Kv1.1-1.8 whose members share 60-74 % sequence identity and identical topology. Kv1 channels are tetrameric proteins with four-fold symmetry around a central potassium ion-selective pore domain. Each protomer has a large cytoplasmic domain (T1) and six transmembrane helices (S1-6)[9]. The voltage-sensing domain (VSD) is formed by S1-4, while S5 and S6 define the pore domain. The region connecting S5 and S6 harbours the pore-forming loop (P-loop), which is further segmented into turret, pore-helix, selectivity filter and pre-S6-loop. Cellular depolarization leads to structural reorganization of the VSD through a stretch of positively charged residues on S4 helices. This triggers movement of the S6 helix and opening of the internal gates, hereby allowing potassium ions into the central cavity to contact with the selectivity filter, which facilitates ion efflux[10,11]. For Kv1.3, sustained channel activation results in so-called C-type inactivation through disruption of key hydrogen bonding between Tyr^{447} to Thr^{441} and Asp^{449} to Trp^{436} in the pore region, which flips main chain carbonyls of selectivity filter residues effectively hindering potassium ion coordination and effective efflux[10,11]. A mechanism exemplified by comparison of the WT Drosophila Kv channel Shaker[12] and the Shaker channel carrying C-type stabilizing mutation W434F[13].

Given its potential relevance as a therapeutic target, subtype-specific pharmacological inhibition of Kv1.3 has been sought, and both peptide-based and small molecules have been developed[6,14] (Figure 1). These include the toxin-derived Shk-peptide Dalazatide (**1**) isolated from the sea anemone *Stichodactyla helianthus*, which functions as a pore-blocker with

picomolar Kv1.3 inhibitor activity and ~100-fold selectivity over Kv1.1 and even higher selectivity (250-2000-fold) towards the remaining Kv1 subtypes[15]. Similarly, Fab-Shk/MNT-002 is a pore-blocking peptide where ShK is fused into the CD3 region of an IgG antibody scaffold[10]. A019009G009 is a nanobody with Kv1.3 inhibitor activity in the nanomolar range[10]. While several selective peptide inhibitors of Kv1.3 has been developed, limited selectivity has been observed for small molecule inhibitors. In this context, the small molecule PAP-1 (**2**) inhibits Kv1.3 with nanomolar potency and has reported 23-125-fold selectivity towards the remaining Kv1 subtypes[16]. Notably, Unterweger et al. described the small molecule inhibitor DES1 which was reported to have nanomolar Kv1.3 potency and more than 1000-fold selectivity towards Kv subtypes 1, 2, 5 and 7[17]. The chemical structure of the highly selective compound was, however, not disclosed.

Structural studies have demonstrated that Fab-Shk/MNT-002 and Dalazatide (**1**) engage residues in the P-loop and selectivity filter and functions as pore blockers by effectively blocking potassium ion efflux with a critical Lys side chain engaging into the selectivity filter [10,18]. The nanobody A019009G009 engages and bridges the turret and VSD domain and captures the selectivity filter in a dilated inactive conformation[10]. Computational modeling and mutagenesis studies suggest that PAP-1 binds Kv1.3 near the P-helix in the central cavity in a 2:1 stoichiometry[19]. However, no experimental structures of Kv1.3 bound to small molecule inhibitors are available, leaving open the critical question of how these molecules bind and the conformational states they stabilize.

To address this knowledge gap, we prepared and characterized selected dichlorophenol Kv1.3 inhibitors from patent applications filed by authors describing DES1. We applied pharmacophore based virtual screening approach to identify a novel indole-based series of highly selective Kv1.3 inhibitors with very high sub-type selectivity. We explored the basic structure activity relationship for this series eventually generating a high potency compound

suitable for cryoEM studies. Using a combination of site-directed mutagenesis and cryoEM we identified the binding site and described the binding modes of the dichlorophenol and indole series. Structural analysis revealed that dichlorophenol and indole series bind Kv1.3 at an extracellular exposed cryptic pocket which is not formed in available Kv1.3 structures. Surprisingly, inhibitor binding at this site modulates the selectivity filter and stabilize a C-type inactive channel conformation. All together this study provides the first atomic-level characterisation of selective Kv1.3 small molecule inhibitors providing in depths understanding of binding modes, subtype selectivity, inhibitory mechanism and enables structure-based drug-design for voltage-gated ion channels.

Results

Identification of novel selective Kv1.3 inhibitors and elucidation of basic structure-activity relationship

To assess potency and selectivity of novel Kv1.3 blockers compared to literature compounds we have measured IC_{50} values in an automated whole-cell patch clamp assay for literature and novel compounds for the eight subtypes of the Kv1 channel family and is reported in Table 1 and Supplementary Figure 1. Compound structures are outlined in Figures 1.

The data for the reference peptide Dalazatide (**1**) is in accordance with literature data[20] whereas the Kv1.3 potency for PAP-1 (**2**) is a factor of 10 weaker compared to the literature[16]. Consequently, the selectivity of PAP-1 (**2**) for Kv1.3 relative to the other Kv1 family members is lower compared to literature data[16].

To obtain structural insight into chemical matter related to the selective blocker DES1[17], we selected two dichlorophenol compounds **3** and **4** for synthesis and testing from patent WO2022076285, which was filed by D. E. Shaw Research that published DES1. The enantiomers of the two dichlorophenol compounds **3** and **4** were separated from racemic mixtures. The absolute stereochemistry was not determined, but according to the patent

publication, the S-enantiomer is the most potent enantiomer. The eutomer **3a** showed potency of 7.9 nM at Kv1.3 with >3,000-fold selectivity over the other seven Kv1 channels. The distomer **3b** showed 2.3-fold lower potency on Kv1.3 with >1,000-fold selectivity (Table 1). These results confirm the high potency and selectivity reported for a proposedly structurally similar compound to DES1[17]. In addition, an analogue with improved affinity/solubility ratio relevant for cryoEM was synthesized. The most potent enantiomer, **4**, showed similar potency and selectivity as **3a**.

To identify structurally novel chemical scaffolds that retain the biological activity of the potent and selective dichlorophenol Kv1.3 inhibitor **3a**, virtual screening was performed. Chemical structures and activity data of Kv1.3 inhibitors reported in the patent WO2022076285 were extracted to generate a 3-D pharmacophore (PHA) model for virtual screening (Figure 2). The PHA model and the S-stereoisomer configuration of **3** were used as a query in the similarity-based scoring in the Enamine HTS Collection small molecule library (https://enamine.net). Shape and electrostatic similarity-based evaluation of the PHA hits by ShaEP [21] identified the dichloroindole **5** as the top-scoring virtual screening hit with a similarity score of 0.6675 when using the S-stereoisomer configuration of dichlorophenol **3** as a query. The identified dichloroindole **5** has a potency of 828 nM at Kv1.3, with >200-fold selectivity over the other seven Kv1 channels.

A set of analogues of the dichloroindole **5** was prepared to explore the structure-activity relationship and to identify a derivative with optimal properties for cryoEM structural elucidation. Replacement of the pyrrolidinecarboxamide group in **5** with a piperazinone moiety (**6a**) enhanced the potency by a factor of 2.7 while retaining the high selectivity. Removal of the two chloro substituents (**6b**) as well as substituting the indole nitrogen atom (**6c**) with a methyl group resulted in a loss of Kv1.3 inhibition (IC_{50}>10,000 nM). Replacement of the chloro substituent in the indole R^3 position in **6a** with a fluoro substituent

in **6d** resulted in a 20-fold Kv1.3 potency reduction. Optimization of the substituents in the indole moiety resulted in (**6e**), with 4-chloro-3,5-difluoro-substitution, exhibiting 78.4 nM potency at Kv1.3. Further replacement of the piperazinone moiety with appropriately substituted *N*-piperazines resulted in **7** with physicochemical properties suited for cryoEM studies and a potency of 13.4 nM at Kv1.3 with >1,500-fold selectivity over the other seven Kv1 channels.

Binding site mapping by mutagenesis

To investigate the structural basis for selectivity, we performed pairwise sequence alignment between Kv1.3 and the remaining Kv1 channels to identify regions with high sequence divergence (Figure 3). Sequence alignment revealed the VSD and P-loop sites as candidate regions possessing high sequence divergence between Kv1.3 and the remaining Kv1 channels. The VSD site is centred at Thr^{322} in the VSD on the loop connecting S2 and S3 (figure 3A and B) whereas the P-loop site is located on the extracellular side at the P-loop spanning the turret and the pre-S6-loop (Figure 3A and C). Kv1.5 was chosen as representative member of the remaining Kv1 family for the generation of chimeric variants, given that PAP-1 (**2**) exhibited inhibition of this channel while Dalazatide (**1**) showed no measurable inhibition (Table 1). We generated stable cell lines expressing Kv1.3 ↔ Kv1.5 chimeric proteins where residues corresponding to site VSD ($Kv1.3^{Kv1.5\ VSD}$, $Kv1.5^{Kv1.3\ VSD}$) (Figure 3B) and site P-loop ($Kv1.3^{Kv1.5\ P\text{-}loop}$, $Kv1.5^{Kv1.3\ P\text{-}loop}$) (Figure 3C) were swapped. Potency measured as IC_{50} values in an automated high-throughput patch-clamp assay for selected inhibitors is reported in Table 2 and Supplementary Figure 2.

In addition to **1**, both the dichlorophenol **3a** and indole **6a** exhibited unchanged potency for $Kv1.3^{Kv1.5\ VSD}$ relative to Kv1.3 WT while potency was abolished for $Kv1.3^{Kv1.5\ P\text{-}loop}$. As expected, **1**, **3a** and **6a** were inactive against Kv1.5 WT, but remarkably, these selective inhibitors all gained activity towards Kv1.5 carrying Kv1.3 site P-loop ($Kv1.5^{Kv1.3\ P\text{-}loop}$). The

potencies of **2** toward Kv1.3 and Kv1.5 were unaffected by the domain swaps, thus serving as a control for the functional expression of chimeric channel variants. Notably, Kv1.3 potency for **2** was 63 nM and selectivity over Kv1.5 was 4.1-fold in line with data presented in Table 1. In summary, mutagenesis studies identify the P-loop of Kv1.3 as the binding site for the Shk-based inhibitor Dalazatide (**1**), dichlorophenol **3a**, and indole **6a**, but not PAP-1 (**2**).

CryoEM structures of human Kv1.3 in complex with either 4 or 7

As a next step, purified full length human Kv1.3 was subjected to single particle cryoEM analysis in complex with dicholorephenol **4** and the indole **7** yielding reconstructions at 2.95 and 2.82 Å resolution, respectively (Supplementary Figure 3 and 4 and Supplementary Table 1). Intracellular T1 domain and the TMD were well resolved while loops 261-290 and 348-358 were poorly defined and thus excluded from the final models. Both structures were very similar to each other (RMSD: 0.22 Å) and to available structure on PDB of Kv1.3 (RMSD: 0.4 – 1.4 Å). Three potassium ions were resolved in the selectivity filter in positions S1, S3 and S4 in both structures (Figure 4E and G) and Tyr^{447} adopted two alternative rotamers in both complexes (Supplementary Figure 5). For both ligand-channel complexes, additional unambiguous density was observed at each protomer near the P-loop consistent with four ligands bound per biological Kv1.3 tetramer (Figure 4B, F, D and H).

Dichlorophenol **4** and indole **7** occupy an extracellular facing pocket, located in the P-loop, sandwiched between the turret and the pre-S6 loop (Figure 5 and 6). The indole and phenol rings are inserted into a hydrophobic cavity formed by Tyr^{447}, Trp^{437}, and Met^{450} as well as Trp^{436} (W^{436B} in Figure 6B and C) situated in the adjacent protomer. The aromatic cores are stabilized through π-stacking with Phe^{428}, while the halogen substituents fill the pocket floor, together orienting the phenol OH in **4** or indole NH in **7** towards Glu^{420}, which forms a favourable hydrogen bond through its sidechain. The chloro substituent in the indole 4-position or phenol *meta* position, are oriented to engage in a potential halogen-bond with the

side chain of Tyr^{447} (Figure 6B and D). For **4**, the lactam carbonyl form a hydrogen bond with the backbone NH of Gly^{427}, which is flipped relative to the Kv1.3:**7** complex. This creates additional space for the shorter link to the terminal amine to form a salt bridge with Asp^{433}. By contrast, the *N*-substituent on the piperazine of **7** was poorly defined (Figure 4H), consistent with substantial conformational flexibility and thus only a tentative placement was modelled aided by computational methods.

To assess the conformational flexibility and dynamic protein:ligand interactions of **7**, a 100 ns molecular dynamics simulation was performed. Root mean square fluctuation (RMSF) analysis revealed pronounced mobility of the terminal azetidine moiety, with values exceeding 4.0 Å for the nitrogen atom, 3.7 Å for the two α-carbons, and 3.1 Å for the β-carbon. Consistent with this high flexibility, the initial salt-bridge interaction between Asp^{433} and the positively charged azetidine moiety was rapidly lost during the simulation and was not re-established, highlighting the transient character of the interaction (Supplementary Figure 11).

For both **4** and **7**, the VSDs were in the polarized configuration (Supplementary Figure 6) and the internal gates in the open state (Supplementary Figure 7) suggesting an activated channel conformation. To understand the inhibitory mechanism, we inspected the selectivity filter and compared this with structures of the active conducting conformation of the Drosophila Kv channel Shaker[12] (PDBid 7SIP) and Kv1.3 in complex with Fab-Shk/MNT-002[10] (PDBid 7SSV) as well as Shaker carrying W434F mutation [13] (PDBid 7SJ1) representing the C-type inactive conformation.

The active conducting conformation defined by structures of Shaker and Kv1.3 in complex with MNT-002 is characterized by main chain carbonyls positioned to accommodate potassium ion coordination along the selectivity filter (Figure 7A1 and A2). This conformation is stabilized by key H-bonds between Asp^{449} (Asp^{447} in Shaker) with Trp^{436}

(Trp^{434} in Shaker) and Tyr^{447} (Tyr ^{445} in Shaker) with Thr^{441} (Thr^{439} in Shaker) (Figure 7B1, B2, C1 and C2). In the C-type inactive conformation, these bonds are broken, and Tyr and Asp side chains point towards the solvent resulting in flipping main chain carbonyls and expansion of the selectivity filter (Figure 7A3, B3 and C3 and Supplementary Figure 10). Upon binding of either **4** or **7**, H-bond between Asp^{449} and Trp^{436} is broken and Asp^{449} moves ~6 Å pointing towards the solvent (Figure 7B4 and B5). Tyr^{447} moves ~12Å and adopts two distinct rotamers (rot1 and 2 in Figure 7C4). Rot1 engages H-bond with Trp^{436} from the neighbouring Kv1.3 protomer (W^{436B} in Figure 7C4) while rot2 points towards solvent in a comparable position to the C-type inactive conformation of Shaker (compare Figure 7C3 and C4). Common for both rotamer conformations is main chain carbonyl flipping (Figure 7A4 and A5). Consequently, the external part of the selectivity filter expands, consistent with lack of potassium ions at position S2. Altogether, the cryoEM analysis showed that **4** and **7** binds Kv1.3 in a cryptic pocket in the P-loop and stabilize a selectivity filter conformation resembling the C-type inactive state.

Discussion

In this study we present the first atomic level characterization of small molecules binding to human Kv1.3. Mutagenesis and cryoEM studies demonstrate that the novel, potent and highly selective yet chemically distinct small molecule inhibitors dichlorophenol (**4**) and indole (**7**) series bind to the P-loop of Kv1.3, which represents one of the few regions that is not conserved across Kv family members. While nanobody A0194009G09, Dalazatide and Fab-ShK/MNT-002 also engages the P-loop, the small molecules bind in a distinct manner. Our data identifies an induced-fit binding mechanism which stabilizes Kv1.3 in a C-type inactive conformation.

Ligand-based virtual screening approach seeded from a patent-described dichlorophenol scaffold identified a novel indole based chemotype **5** as selective Kv1.3 inhibitors. Based on the alignment model of **3a** and **5**, the indole NH overlap with the phenol OH preserving hydrogen bond donor function while the dichloro substituent aromatic systems are also well aligned. Lactam group of **3a** is mimicked by a carbonyl-pyrrolidine moiety in **5** providing a relatively close alignment between the amide groups (Figure 2B). These considerations are supported by structure activity relationships for analogues of the novel indole **5** (Figure 1 and Table 1). The experimental data indicate an essential role of the indole NH as well as the 4,5-dichloro-subsituents for activity. Removal of the two chloro substituents (**6b**) as well as substituting the indole nitrogen atom (**6c**) with a methyl group in the piperazinone analogue **6a** resulted in loss of Kv1.3 potency. Based on this insight, further structure activity relationship investigations led to the novel indole derivative **7** with nanomolar Kv1.3 potency and >1,500-fold selectivity towards the other seven Kv1 channels. Due to the attractive Kv1.3 potency and selectivity as well as high solubility **7** was selected as indole representative for cryoEM studies.

Mutagenesis experiments conducted to structure determination identified the binding region of both dichlorophenol and indole series near the P-loop. Dalazatide (**1**), dichlorophenol (**3a**) and indole **6b** showed identical binding profiles as potencies were abolished in $Kv1.3^{Kv1.5\ P\text{-}loop}$ and introduced in $Kv1.5^{Kv1.3\ \text{-}P\text{-}loop}$ showing that inhibitors function by engaging residues in P-loop (Figure 3 and Table 2). This agrees with cryoEM studies for close analogue of **1**[10] and showed that small molecules **3a** and **6b** bind Kv1.3 at similar site as the peptide blocker Dalazatide (**1**).

The cryoEM structures confirmed the identified binding location and further revealed atomic description of ligand binding modes. Surprisingly, both chemotypes occupy a novel pocket that is not present in published Kv1.3 structures (Supplementary Figure 8 and 9), suggesting

an induced-fit binding mechanism into a cryptic pocket. The highly dynamic and flexible character of the P-loop was previously observed and two subunit conformations, dilated 1 (D1) and dilated 2 (D2), were shown to co-exist in cryoEM[10]. In our structures, the P-loop movement is restricted, though not abolished, by **4** and **7**, as revealed by a slight decrease in side-chain definition of the cryoEM map at the P-loop.

Most residues in the binding pocket are conserved across Kv1 family members while the turret is sequence divergent within the Kv1 family (Figure 3C and 6). The turret defines the binding pocket roof and for other Kv1 family members amino acid at position 427 is a bulky residue (His/Glu/Leu) that is a Gly in Kv1.3. Based on these findings we propose that Kv1.3-specific features i.e. Pro^{424} combined with smaller downstream residues Thr^{425}, Ser^{426} and Gly^{427} enable the turret to adopt conformations favouring ligand binding and thus governing the observed sub-type specificity for both the dichlorophenol and indole series.

Despite being structurally distinct, dichlorophenol (**4**) and the 4-chloro-3,5-difluoroindole (**7**) bind in an almost identical manner (Figure 5 and 6). A crucial interaction for both scaffolds is a hydrogen bond formed between the phenol OH or indole NH and the side chain of Glu^{420}. In addition, the halogen substituted aromatic systems extend into a predominantly hydrophobic cavity, while the *N*-substituent on the piperazine of **7** extends toward solvent. The structure–activity relationships for close analogues are consistent with this binding mode as potency requires precise orientation of halogens and a hydrogen bonding donor on the core scaffold, whereas the solvent exposed moity tolerates significant modification. Additionally, it is likely that the chlorine atom at position R^3 on **7** forms a halogen-bond with the side chain of Tyr^{447} as substitution at this position to a fluoro substituent for close analogues (**6a** vs **6d**) resulted in a 20-fold drop in potency (Table 2). Together, these insights provide a solid rational for future optimization efforts.

Our structural analyses reveal that inhibitor binding stabilizes a conformation of Kv1.3 with dilated selectivity filter where main-chain carbonyls are flipped and unable to coordinate potassium ions (Figure 7 and Supplementary Figure 10). The dilated conformation shows disruption of two key hydrogen bonds characterizing the active conducting channel conformation. Consequently, the selectivity filter adopts a conformation resembling Shaker W434F representing a C-type inactive state[13]. However, Kv1.3 Tyr^{447} adopts two distinct rotamer conformations, where rotamer1 engages in a novel H-bond with Trp^{436B} and also forms the bottom of the hydrophobic binding pocket forming halogen bonding with ligand chloride atoms, further increasing the energetic barrier to potassium ion permeation. This, together with the observation that the S4 helix is in the polarized/activated conformation (Supplementary Figure 6) and that the inner gates are open (Supplementary Figure 7), suggests that **4** and **7** capture Kv1.3 in a C-type inactive conformation thus potentially binding in a state-dependent manner. The inhibitory state of the selectivity filter resembles that induced by the nanobody A0194009G09[10], as identical key H-bonds are broken resulting in a widening of the selectivity filter (Supplementary Figure 10). Interestingly, Tyr^{447} also adopts two rotamers upon nanobody binding further highlighting the structural flexibility of this key residue. This mechanism is in sharp contrasts to Dalazatide (**1**) and Fab-ShK/MNT-002 which stabilize the open-active selectivity filter conformation by inserting a Lys side chain in the potassium ion S1 site thus acting as a direct pore-blocker. The described inhibitory mechanism for dichlorophenol (**4**) and indole (**7**) adds to the repertoire of pharmacological blocking mechanisms available for Kv1.3. With these new tools it is now possible to compare open-channel pore-blocking with allosteric C-type inhibition on downstream physiological effects and to assess the therapeutic potential of specific Kv1.3 inhibition.

Structural studies of pH-dependent potassium ion channel KcsA and Kv channels in complex with activators and inhibitors have highlighted many different binding sites and mechanisms utilized by these modulators before (summarized in Figure 8, for comprehensive reviews, see refs. [6,22]). Besides nanobody A0194009G009, toxin-blockers and now compounds **4** and **7** which engage the channel at the extracellular side, these include 1) binding to the central cavity and blocking potassium ion engagement with the selectivity filter[23] 2) activation by modulation of channel fenestration[24,25], 3) activation by binding to the VSD and stabilizing the activated state [26] 4) binding below the internal gates and blocking potassium entry into the central cavity[27] and finally 5) by modulating activity of accessory intracellular proteins[2828]. In summary, the results presented in this study are, to our knowledge, the first to report small molecule inhibitors working via allosteric modulation of the selectivity filter through the P-loop, a site previously restricted to peptide-based inhibitors. These findings expand the mechanistic repertoire of Kv channel pharmacology, establish atomic level principles underlying Kv1.3 subtype selectivity, and offer a foundation for rational design of next generation therapeutics targeting Kv1.3 and potentially other voltage gated potassium ion channels.

Methods

Protein expression and purification

Full-length human Kv1.3 carrying a 3C cleavage site followed by a C-terminal GFP and Strep-tag was expressed by transient transfection in HEK293 GnTI– cells. Cells were transfected using PEI and grown in FreeStyle medium supplemented with 2% FBS at 2×10^6 cells/mL. Transfected cells were incubated for 24 h at 37°C, 5% CO_2, followed by 48 h at 30°C, 5% CO_2. Cell pellets were harvested, flash-frozen in liquid nitrogen, and stored at –80°C. Pellets were homogenized in 50 mM Tris-HCl pH 7.5, 150 mM KCl, 2 mM $MgCl_2$, 2 mM DTT, 1% DDM, and 0.1% CHS, supplemented with protease inhibitor tablets (Roche), Pefabloc, and DNase I (10 µg/mL) by gentle dounce homogenization and incubated for 30 to 60 min to promote membrane solubilization. Solubilized fraction was recovered by ultracentrifugation at 100,000×g for 30 min and incubated with homemade anti-GFP affinity resin for 2 h. The resin was washed extensively with Work buffer (50 mM Tris-HCl pH 7.5, 150 mM KCl, 0.025% DDM, 0.0025% CHS), including an initial wash containing 5 mM ATP to remove potential chaperone contaminants. Bound protein was eluted by on-resin cleavage using an excess of HRV 3C protease (estimated 1:2 w/w) for 2 h. The cleaved, tagless Kv1.3 was concentrated by spin-centrifugation and subjected to size-exclusion chromatography on a Superose 6 Increase 10/300 GL column in Work Buffer. The peak of interest eluting at 14.4 mL was pooled, concentrated to 5 mg/mL, and used for cryo-EM grid preparation. Final protein amounts were typically around 75 µg/L culture.

Cryo-EM sample preparation and data acquisition

Freshly purified protein was used for cryo-EM grid preparation. The protein was concentrated to 3.5 or 5 mg/mL and incubated with 1 mM compound **4** or **7** prior to vitrification. Three microliters of sample were applied to pre-glow-discharged Quantifoil R1.2/1.3 Au 300 mesh grids and blotted for 3s using a Leica EM GP plunger operated at

10°C and 85% relative humidity. For the **4** complex, 22'757 micrographs were collected on a Titan Krios transmission electron microscope operated at 300 kV, equipped with a Selectris energy filter and a Falcon 4i direct electron detector. Data were acquired at a nominal pixel size of 0.926 Å, with a total electron dose of 50 $e^{-}/Å^{2}$ fractionated over 50 frames, and a defocus range of -0.5 to -3 µm.

For the **7** complex, data were collected under identical conditions, except that 35'700 micrographs were acquired at a nominal pixel size of 0.726 Å and a dose of 60 $e^{-}/Å^{2}$.

Structure determination refinement and validation

Cryo-EM data processing was performed using cryoSPARC v4.4. For both complexes, dose-fractionated movies were motion-corrected using Patch Motion Correction, and contrast transfer function (CTF) parameters were estimated using Patch CTF Estimation. Micrographs were manually inspected and curated to remove poor-quality images. Particles were initially picked using a blob-based picker, followed by iterative rounds of 2D classification and 3D classification to identify well-resolved particle populations.

For **4** complex, selected particles were further refined using a combination of heterogeneous refinement, non-uniform refinement, and local refinement. This resulted in a final stack of 127'851 aligned particles, extracted with a 360-pixel box size, yielding a cryo-EM map at 2.95 Å resolution, as estimated by the gold-standard Fourier shell correlation (FSC) criterion at 0.143. The particle stack was then subjected to local focused refinement using soft masks around the transmembrane domain and the T1 domain, resulting in two additional cryo-EM maps at 2.87Å and 2.89Å, respectively. C4 symmetry was applied during refinement after confirmation in C1 that symmetry application was appropriate.

For the **7** complex, an analogous processing strategy was applied, resulting in a final stack of 277'705 aligned particles, extracted with a 420-pixel box size, and yielding a cryo-EM map at 2.79 Å resolution (FSC = 0.143), as well as two local focused refined maps at 2.66Å and

2.82Å for the transmembrane and T1 domains respectively.

A schematic representation of the processing workflow is provided in Supplementary Figure 3 and Supplementary Figure 4.

For both structures, the D2 subunit conformation was identified as the predominant state; accordingly, PDBid 7SSY was used as the starting model for atomic model building. Model refinement was performed through iterative cycles of manual model building in Coot v0.9.8.7 and real-space refinement using phenix.refine v1.21.2. Geometry restraints for both ligands were generated using phenix.elbow. Figures were prepared in Chimera or Pymol.

Molecular dynamics simulations

Protein and ligand structures were prepared at pH 7.4 using the Protein Preparation Wizard implemented in Maestro (release 2024-1, Schrödinger, LLC, New York, NY, USA). Molecular dynamics simulations were performed using the Desmond simulation package[29]. The system was embedded in a POPC membrane environment and aligned according to the Orientations of Proteins in Membranes (OPM) [30] database entry for PDB ID 7SSY. Solvation was carried out using the TIP3P water model in an orthorhombic simulation box, and the OPLS4 force field was applied to all components. Analyses were performed on chain A of the ligand–protein complex and included ligand RMSF, ligand torsional profiles (Supporting Information), and ligand–protein interaction analysis. To allow for system equilibration, only the final 40 ns of the simulation trajectory were included in the analysis.

Virtual screening

Virtual screening (VS) was employed to identify novel inhibitors of Kv1.3. As the exact binding site of the known inhibitors was not reported at the time, a ligand-based VS was performed with the goal of identifying structurally novel scaffolds that retain the biological activity of known Kv1.3 inhibitors.

Chemical structures and activity data of Kv1.3 inhibitors reported in the patent WO2022076285 were extracted to generate a 3D-pharmacophore (PHA) model for VS. In the patent, compounds were classified into five groups based on Kv1.3 IC_{50} [μM]: < 0.01, < 0.1, < 1, < 10, and < 30. Molecules that lacked activity data and two molecules with undefined chiral centers were dropped out. Prior to PHA model generation, the ligands were prepared using LigPrep module in Maestro (release 2022-1, Schrödinger, LLC, New York, NY, USA). Protonation states at pH 7.4 were predicted with Epik[31,32] and 3D-conformations and partial charges were assigned using the OPLS4 force field[33]. For chiral compounds, the stereoisomer described in the patent was generated.

3D-alignment of the patent compounds and PHA model generation was done using Phase implemented in Maestro[34,35]. Compounds with IC50 >= 10 μM were defined as inactive. The model was required to fit to at least 30% of the actives and contain maximum of two hydrophobic features. A PHA model with six features was obtained: two hydrogen bond acceptors, one hydrogen bond donor, two hydrophobic sites, and one aromatic ring (Figure 3A). Tolerance of 2 Å was used with each pharmacophoric feature for fitting ligands to the model.

VS was performed with the Enamine HTS Collection small molecule library (https://enamine.net). The library was prepared using the same protocol as for the patented Kv1.3 inhibitors, with the exception that all possible stereoisomers were generated for compounds with undefined stereochemistry. Prior to pharmacophore screening, the library was pre-filtered with the following criteria: molecular weight 250-550 Da, <9 rotatable bonds, logP < 5.7 (calculated with QikProp, release 2022-1, Schrödinger, LLC). Finally, sets of 3D-conformations were generated for each compound in the library using ConfgenX of the Schrödinger package (release 2022-1, Schrödinger, LLC). The virtual library was screened to identify potential hit compounds based on their 3D-alignment with the pharmacophoric

features described by the PHA model. The compounds identified in PHA screening were further scored by shape- and electrostatic similarity using the program ShaEP[21]. Rescoring VS hits with ShaEP has been shown to improve early enrichment of active molecules in VS campaigns with a variety of target proteins[36–40]. Ex 56 (S-stereoisomer of **3**) described in the patent was used as a query in the similarity-based scoring. VS hits were visualized using Bodil[41]. Figures were generated using either Maestro or PyMOL (version 2.5.0, Schrödinger, LLC).

Kv1.3 and Kv1.5 cells lines

Stable cell lines harboring wild-type or mutant variant of Kv1.3 or Kv1.5 were generated using the T-REx™ CHO system (Thermo Fisher Scientific). Plasmids encoding mutant variants were generated by molecular cloning services (GeneArt) and inserted into pJTI R4 CMV-TO MCS pA vector. CHO-K1 Jump-In T-REx cells were stably transfected by lipofection. After 24h of incubation, appropriate antibiotic selections (5 mg/mL G418 + 10 µg/mL Blasticidin) were added to the cells and stable isogenic pools were obtained after approximately 15 days.

Electrophysiology

Functional activity on Kv1.3 WT was tested by automated patch clamp in a Qpatch system (Sophion, Denmark) in whole cell configuration using a single hole chip. Extracellular solution composition was (in mM): 145 NaCl, 5 KCl, 1 $MgCl_2$, 2 $CaCl_2$, 10 HEPES and 10 glucose, pH 7.4. Intracellular composition was (in mM): 20 KCl, 120 KF, 10 HEPES, 10 EGTA, pH 7.2. Inhibitor molecules were tested in cumulative dose-response at a final DMSO concentration of 0.1% in extracellular solution. Currents were elicited by voltage step to -30 mV from a holding potential of -90mV. Intersweep interval was 15 s and sampling rate 5kHz. The averaged steady-state currents and charge level at the end of the compound application were measured and normalized to the maximum current response in the vehicle period. To

obtain the IC_{50} values, the normalized data were plotted against the respective inhibitor concentrations on a logarithmic scale and fitted with sigmoidal dose-response curve in PRISM GraphPad software. IC_{50} values were only estimated if % of inhibition at the highest tested concentration were greater than 50%.

Activity on Kv1.x channels was tested by automated patch clamp analysis using QPatch 48 following a similar setup as described for Kv1.3 with the following exceptions: Extracellular solution composition was (in mM): 156 NaCl, 4 KCl, 1 $MgCl_2$, 3 $CaCl_2$, 10 HEPES and 10 glucose, pH 7.4; Intracellular solution contained (in mM): 20 KCl, 120 KF, 10 HEPES, 10 EGTA, Na_2ATP 5, pH 7.2. Currents were elicited by a 500 ms voltage step from -80mV to +30mV. Inhibitors were applied at a final DMSO concentration of 0.3% DMSO v/v.

Activity on Kv1.3 WT, Kv1.5 WT, $Kv1.3^{Kv1.5\ P\text{-}loop}$, $Kv1.3^{Kv1.5\ VSD}$ $Kv1.^{5Kv1.3\ P\text{-}loop}$ and $Kv1.5^{Kv1.3\ VSD}$ was assessed by automated patch clamp using a SyncroPatch 384 system (Nanion, Germany). 24 hours prior to the experiment, cellular Kv1.3 expression was induced with doxycycline. Extracellular solution composition was (in mM): 140 NaCl, 4 KCl, 1 $MgCl_2$, 2 $CaCl_2$, 10 HEPES and 5 glucose, pH 7.4; Intracellular solution contained (in mM): 110 KF, 10 KCl, 10 EGTA, 10 HEPES, pH 7.2. Vehicle for addition of inhibitors consisted of extracellular solution supplemented with 0.1% DMSO and 0.05% pluronic acid. Experiments were performed at room temperature in whole cell configuration using single hole chips at a sampling rate of 5kHz. Holding potential was -90 mV and intersweep interval was 30 s. For functional validation of variant hKv1.3/hKv1.5 cell lines, 750ms steps from -70 mV to + 30mV were applied followed by a single voltage step (100 ms) at -50 mV. For compound testing, currents were elicited by 200 ms depolarizing steps to +30 mVTo obtain the IC_{50} values, the normalized data were plotted against the respective inhibitor concentrations on a logarithmic scale and fitted with sigmoidal dose-response curve in

PRISM GraphPad software. IC_{50} values were only estimated if % of inhibition at the highest tested concentration were greater than 50%.

Chemistry

The compounds used for pharmacological studies and structural elucidations are commercially available or prepared according to the procedures outlined in the supplementary materials.

Data availability

Atomic coordinates for Kv1.3 in complex with **4** and **7** have been deposited in the Protein Data Bank (PDB) under accession codes 30BF (Kv1.3:**4**) and 30ZB (Kv1.3:**7**). The cryoEM maps have been deposited in the Electron Microscopy Data Bank (EMDB) under accession codes EMD-57536 (Kv1.3:**4** Overall map), EMD-57533 (Kv1.3:**4** TM focused),EMD57535 (Kv1.3:**4** T1 focused), EMD-58170 (KV1.3:**7** Overall map), EMD-57753 (Kv1.3:**7** TM focused) and EMD-57754 (Kv1.3:**7** T1 focused).

Acknowledgements

This study was funded by Muna Therapeutics and The Michael J. Fox Foundation for Parkinson's Research. We thank Dubochet Center for Imaging (DCI) Lausanne for their support in cryo-EM data collection. We thank Axxam SPA for support with cell line generation and electrophysiology experimental data collection. We thank Metrion Biosciences for support with electrophysiology on Kv1.x channels Interpretations and conclusions are those of the authors and not necessarily endorsed by DCI, Axxam or Metrion.

Author contributions

J.V., G.W., L.C.R., M.T.P., J.B.P. and K.A. conceptualized the study. J.V., M.T., E.M.J., G.W., M.B., F.D., C.P.S., O.T.P., M.H., J.B.P. and K.A. performed experiments, acquired and or analysed data. M.T., M.B., F.D., C.P.S. and M.H. performed cryoEM and molecular dynamics experiments. E.M.J. and O.T.P performed virtual screening experiments. G.W., J.B.P. and K.A. designed small molecule inhibitors. J.V., M.T., E.M.J., G.W., L.C.R., M.B., F.D., C.P.S., O.T.P., M.H., J.B.P. and K.A. interpreted data. J.A. and K.A. wrote the manuscript with input from all authors.

Competing interests

J.V., L.C.R., M.T.P., J.B.P. and K.A are all current or former employees of Muna Therapeutics. The remaining authors have no financial interest related to the present study.

Additional information

Supplementary information covering compound synthesis is available.

References

1. Chirra, M. *et al.* How the Potassium Channel Response of T Lymphocytes to the Tumor Microenvironment Shapes Antitumor Immunity. *Cancers* vol. 14 Preprint at https://doi.org/10.3390/cancers14153564 (2022).
2. Ginefra, P., Hope, H. C., Spagna, M., Zecchillo, A. & Vannini, N. Ionic regulation of T-cell function and anti-tumour immunity. *International Journal of Molecular Sciences* vol. 22 Preprint at https://doi.org/10.3390/ijms222413668 (2021).
3. Beeton, C. *et al.* Targeting effector memory T cells with a selective peptide inhibitor of Kv1.3 channels for therapy of autoimmune diseases. *Mol. Pharmacol.* **67**, 1369–1381 (2005).
4. Beeton, C. *et al. Kv1.3 Channels Are a Therapeutic Target for T Cell-Mediated Autoimmune Diseases*. https://www.pnas.org (2006).
5. Wang, X. *et al.* Kv1.3 Channel as a Key Therapeutic Target for Neuroinflammatory Diseases: State of the Art and Beyond. *Frontiers in Neuroscience* vol. 13 Preprint at https://doi.org/10.3389/fnins.2019.01393 (2020).
6. Lopez-Mateos, D., Harris, B. J., Hernández-González, A., Yarov-Yarovoy, V. & Wulff, H. Recent advances in the pharmacology of voltage-gated ion channels. *Pharmacol. Rev.* **77**, 100090 (2025).
7. Wulff, H., Castle, N. A. & Pardo, L. A. Voltage-gated potassium channels as therapeutic targets. *Nat. Rev. Drug Discov.* **8**, 982–1001 (2009).
8. Barros, F., Pardo, L. A., Domínguez, P., Sierra, L. M. & de la Peña, P. New structures and gating of voltage-dependent potassium (Kv) channels and their relatives: A multi-domain and dynamic question. *International Journal of Molecular Sciences* vol. 20 Preprint at https://doi.org/10.3390/ijms20020248 (2019).
9. Liu, S. *et al.* Structures of wild-type and H451N mutant human lymphocyte potassium channel KV1.3. *Cell Discovery* vol. 7 Preprint at https://doi.org/10.1038/s41421-021-00269-y (2021).
10. Swartz, K. J. Sensing voltage across lipid membranes. *Nature* vol. 456 891–897 Preprint at https://doi.org/10.1038/nature07620 (2008).
11. Huang, J., Pan, X. & Yan, N. Structural biology and molecular pharmacology of voltage-gated ion channels. *Nat. Rev. Mol. Cell Biol.* **25**, 904–925 (2024).
12. Selvakumar, P. *et al.* Structures of the T cell potassium channel Kv1.3 with immunoglobulin modulators. Preprint at https://doi.org/10.1101/2022.04.19.488765 (2022).
13. Reddi, R., Matulef, K., Riederer, E. A., Whorton, M. R. & Valiyaveetil, F. I. *Structural Basis for C-Type Inactivation in a Shaker Family Voltage-Gated K + Channel*. *Sci. Adv* vol. 8 https://www.science.org (2022).
14. Tan, X.-F. *et al.* Structure of the Shaker Kv channel and mechanism of slow C-type inactivation. *Sci. Adv.* **8**, (2022).
15. Tan, X.-F. *et al.* Structure of the Shaker Kv channel and mechanism of slow C-type inactivation. *Sci. Adv.* **8**, (2022).
16. Gubič, Š. *et al.* Discovery of Kv1.3 ion channel inhibitors: Medicinal chemistry approaches and challenges. *Med. Res. Rev.* **41**, 2423–2473 (2021).
17. Pennington, M. W. *et al.* Engineering a stable and selective peptide blocker of the Kv1.3 channel in T lymphocytes. *Mol. Pharmacol.* **75**, 762–773 (2009).
18. Schmitz, A. *et al.* Design of PAP-1, a Selective Small Molecule Kv1.3 Blocker, for the Suppression of Effector Memory T Cells in Autoimmune Diseases. *Mol. Pharmacol.* **68**, 1254–1270 (2005).

19. Unterweger, A. L. *et al.* Suppressing Kv1.3 Ion Channel Activity with a Novel Small Molecule Inhibitor Ameliorates Inflammation in a Humanised Mouse Model of Ulcerative Colitis. *J. Crohns Colitis* **15**, 1943–1958 (2021).
20. Tyagi, A. *et al.* Rearrangement of a unique Kv1.3 selectivity filter conformation upon binding of a drug. *PNAS* https://doi.org/10.1073/pnas.2113536119/-/DCSupplemental (2021) doi:10.1073/pnas.2113536119/-/DCSupplemental.
21. Zimin, P. I., Garic, B., Wulff, H. & Zhorov, B. S. Mapping the Binding Site of the Alkoxypsoralen PAP-1 in the Voltage-Gated K+ Channel Kv1.3. *Biophys. J.* **96**, 176a (2009).
22. Tarcha, E. J. *et al.* Durable pharmacological responses from the peptide ShK-186, a specific Kv1.3 channel inhibitor that suppresses T cell mediators of autoimmune disease. *Journal of Pharmacology and Experimental Therapeutics* **342**, 642–653 (2012).
23. Vainio, M. J., Puranen, J. S. & Johnson, M. S. ShaEP: Molecular Overlay Based on Shape and Electrostatic Potential. *J. Chem. Inf. Model.* **49**, 492–502 (2009).
24. Lenaeus, M. J., Burdette, D., Wagner, T., Focia, P. J. & Gross, A. Structures of KcsA in Complex with Symmetrical Quaternary Ammonium Compounds Reveal a Hydrophobic Binding Site. *Biochemistry* **53**, 5365–5373 (2014).
25. Ma, D. *et al.* Structural mechanisms for the activation of human cardiac KCNQ1 channel by electro-mechanical coupling enhancers. *Proceedings of the National Academy of Sciences* **119**, (2022).
26. Willegems, K. *et al.* Structural and electrophysiological basis for the modulation of KCNQ1 channel currents by ML277. *Nat. Commun.* **13**, 3760 (2022).
27. Li, X. *et al.* Molecular basis for ligand activation of the human KCNQ2 channel. *Cell Res.* **31**, 52–61 (2021).
28. Li, T. *et al.* Structural Basis for the Modulation of Human KCNQ4 by Small-Molecule Drugs. *Mol. Cell* **81**, 25-37.e4 (2021).
29. Pan, Y. *et al.* Cortisone dissociates the Shaker family K+ channels from their β subunits. *Nat. Chem. Biol.* **4**, 708–714 (2008).
30. Bowers, K. J. *et al.* Molecular dynamics---Scalable algorithms for molecular dynamics simulations on commodity clusters. in *Proceedings of the 2006 ACM/IEEE conference on Supercomputing - SC '06* 84 (ACM Press, New York, New York, USA, 2006). doi:10.1145/1188455.1188544.
31. Lomize, M. A., Pogozheva, I. D., Joo, H., Mosberg, H. I. & Lomize, A. L. OPM database and PPM web server: resources for positioning of proteins in membranes. *Nucleic Acids Res.* **40**, D370–D376 (2012).
32. Greenwood, J. R., Calkins, D., Sullivan, A. P. & Shelley, J. C. Towards the comprehensive, rapid, and accurate prediction of the favorable tautomeric states of drug-like molecules in aqueous solution. *J. Comput. Aided. Mol. Des.* **24**, 591–604 (2010).
33. Shelley, J. C. *et al.* Epik: a software program for pK a prediction and protonation state generation for drug-like molecules. *J. Comput. Aided. Mol. Des.* **21**, 681–691 (2007).
34. Lu, C. *et al.* OPLS4: Improving Force Field Accuracy on Challenging Regimes of Chemical Space. *J. Chem. Theory Comput.* **17**, 4291–4300 (2021).
35. Dixon, S. L., Smondyrev, A. M. & Rao, S. N. PHASE: A Novel Approach to Pharmacophore Modeling and 3D Database Searching. *Chem. Biol. Drug Des.* **67**, 370–372 (2006).
36. Dixon, S. L. *et al.* PHASE: a new engine for pharmacophore perception, 3D QSAR model development, and 3D database screening: 1. Methodology and preliminary results. *J. Comput. Aided. Mol. Des.* **20**, 647–671 (2006).

37. Niinivehmas, S. *et al.* Blocking oestradiol synthesis pathways with potent and selective coumarin derivatives. *J. Enzyme Inhib. Med. Chem.* **33**, 743–754 (2018).
38. Jokinen, E. M., Postila, P. A., Ahinko, M., Niinivehmas, S. & Pentikäinen, O. T. Fragment- and negative image-based screening of phosphodiesterase 10A inhibitors. *Chem. Biol. Drug Des.* **94**, 1799–1812 (2019).
39. Kurkinen, S. T., Lehtonen, J. V., Pentikäinen, O. T. & Postila, P. A. Optimization of Cavity-Based Negative Images to Boost Docking Enrichment in Virtual Screening. *J. Chem. Inf. Model.* **62**, 1100–1112 (2022).
40. Jokinen, E. M. *et al.* Virtual Screening Strategy to Identify Retinoic Acid-Related Orphan Receptor γt Modulators. *Molecules* **28**, 3420 (2023).
41. Moyano-Gómez, P., Lehtonen, J. V., Pentikäinen, O. T. & Postila, P. A. Building shape-focused pharmacophore models for effective docking screening. *J. Cheminform.* **16**, 97 (2024).
42. Lehtonen, J. V. *et al.* BODIL: a molecular modeling environment for structure-function analysis and drug design. *J. Comput. Aided. Mol. Des.* **18**, 401–419 (2004).

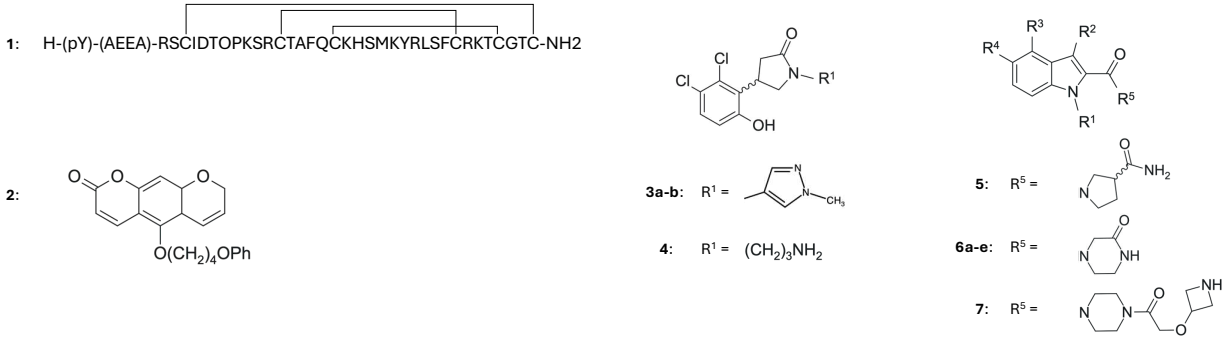


Figure 1. Chemical structures of Kv1.3 inhibitors used in this study. 1: Dalazatide; pY = phosphotyrosine, AEEA = 8-amino-3,6-dioxaoctanoic acid. Solid lines indicates disulfide bonds. **2:** PAP-1 or 5-(4-phenoxybutoxy)psoralen. **3-4:** Chemical structures of dichlorophenol based Kv1.3 inhibitors. Structures of R^1 are shown underneath the core scaffold. **5-7:** Chemical structures of indole based inhibitors. Top structure illustrates core scaffold and groups R^{1-4} are shown in Table 1. Structures of R^5 are shown underneath the core scaffold.

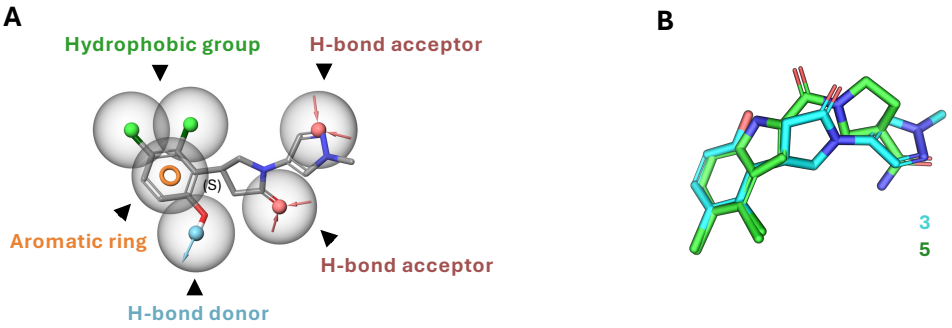


Figure 2. Pharmachophore based virtual screening model and structural alignment of hit and query molecule. A: Pharmacophore model generated from known Kv1.3 inhibitors shown on S-sterioisomer of **3**. The transparent spheres indicate tolerances in fitting a ligand to the model. **B:** 3D-alignment of S-sterioisomer of **3** and hit molecule **5**.

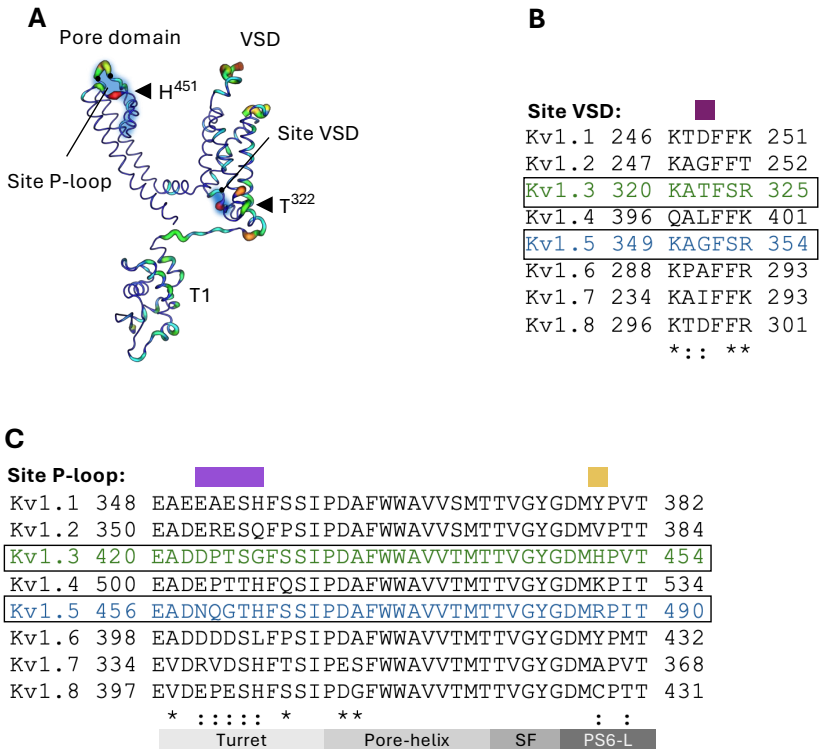


Figure 3. Identification of potential binding site for selective Kv1.3 inhibitors. A: Monomer of Kv1.3 (PDBid 7SSZ) viewed from the side with sites VSD and pore domain. Protein sequence conservation is illustrated by thickness and color i.e. narrow and blue indicates high conservation within the Kv1 family and wide and red indicates residues unique to Kv1.3. Note that His^{451} and Thr^{322} are unique to Kv1.3. **B:** Sequence alignment for site VSD with position of Thr^{322} indicated. **C:** Sequence alignement for site P-loop within the Kv1 family. Colored boxes above figure B and C indicate residues which were evaluated in mutagenesis studies. SF = selectivity filter, PS6-L = pre-S6-loop. Primary sequence of Kv1.3 and Kv1.5 are colored in accordance to Table 2.

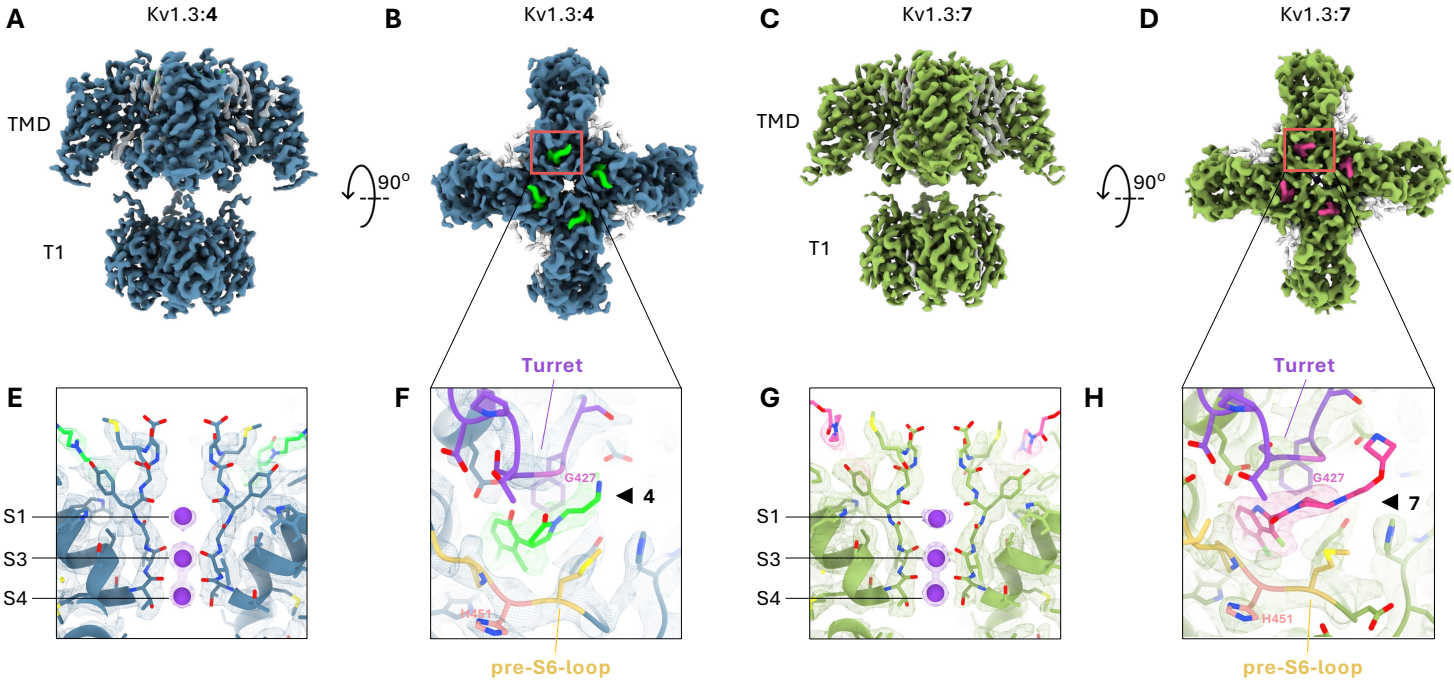


Figure 4. CryoEM structures of human Kv1.3 bound to ligands 4 and 7. A and **C:** CryoEM density map of human Kv1.3 in complex with **4** or **7** viewed from side. **B** and **D:** CryoEM density map of human Kv1.3 in complex with **4** (in green) or **7** (in red) viewed from top. **E** and **G:** CryoEM density map of selectivity filter for Kv1.3 in complex with **4** or **7**. **F** and **H:** CryoEM density map of ligand binding site for **4** or **7**.

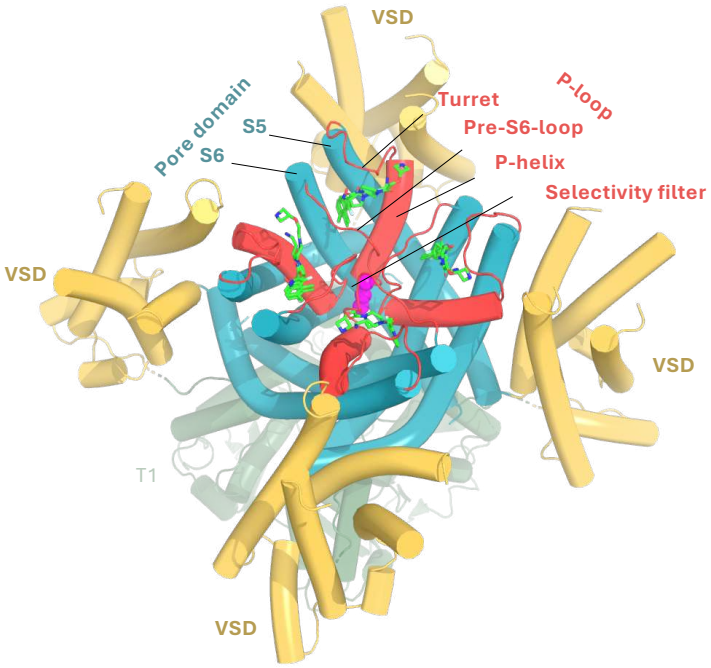


Figure 5. Compounds 4 and 7 bind Kv1.3 in a cryptic pocket at the P-loop. Kv1.3 viewed from top with different domains indicated. Structure of Kv1.3 in complex with compounds **4** and **7** are superimposed and **4** and **7** are are represented as sticks while Kv1.3 is presented as cartoon.

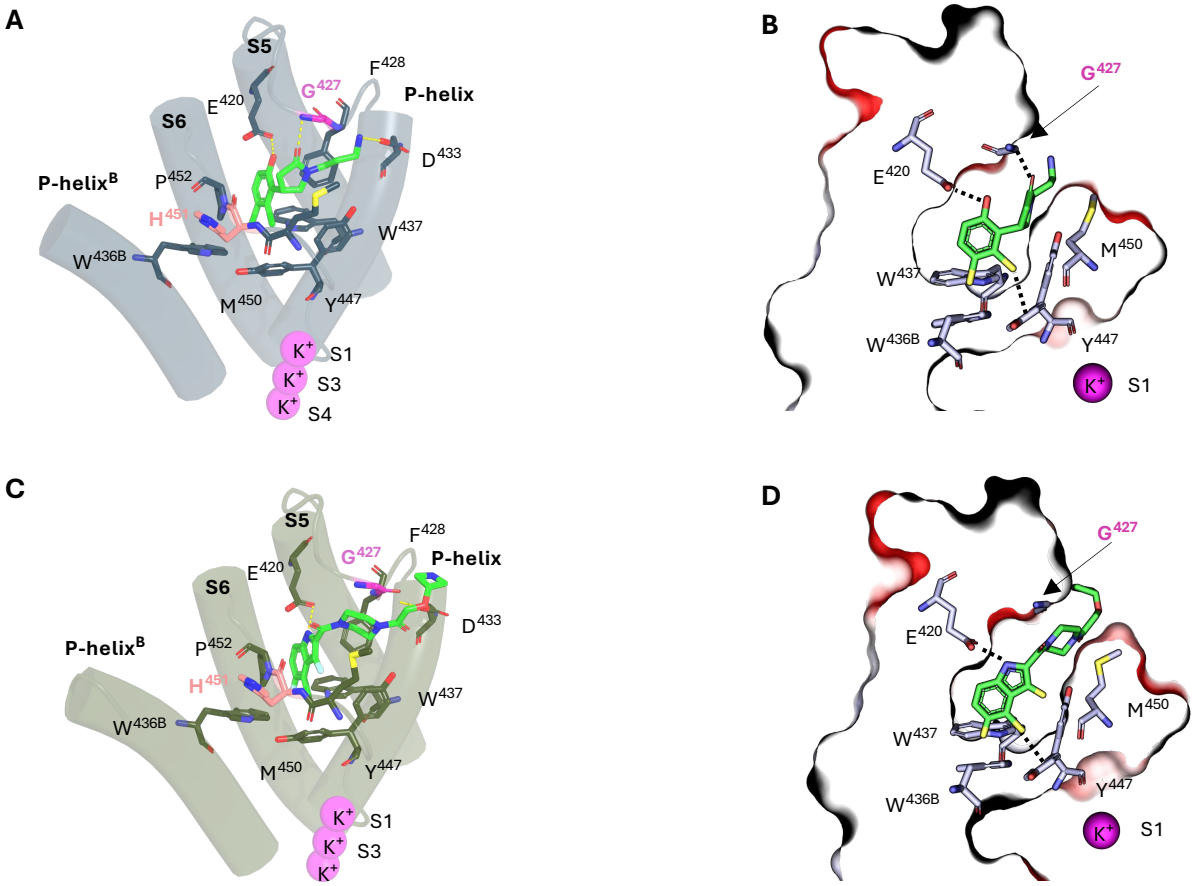


Figure 6. Description of binding site for compounds 4 and 7. A: Binding site for compound **4**. Residues defining the binding are shown as sticks. His^{451} and Gly^{427} were part of the mutagenesis studies are colored in accidence with figure 3. **B:** Side view of binding site for compound **4**. Protein is shown as surface and specific residues are shown as sticks. Dotted lines represent H-bonds or potential halogen bonds. **C:** Binding site for compound **7**. Residues defining the binding are shown as sticks. His^{451} and Gly^{427} were part of the mutagenesis studies are colored in accidence with figure 3. **D:** Side view of binding site for compound **7**. Protein is shown as surface and specific residues are shown as sticks. Dotted lines represent H-bonds or potential halogen bonds.

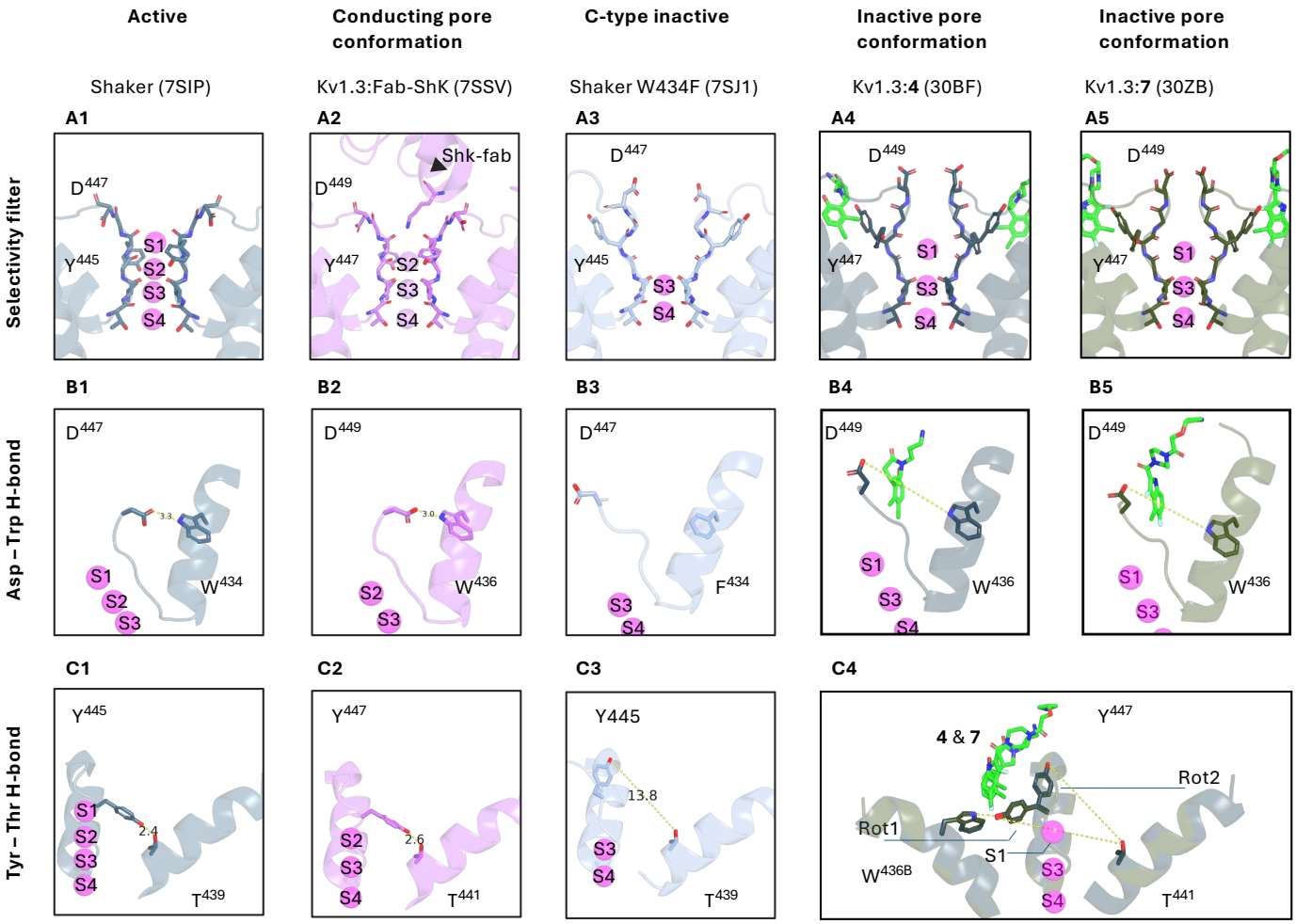


Figure 7. Compound 4 and 7 binding in the cryptic pocket breaks H-bond network chracteristic of active conducting pore conformation. Column 1: Active channel conformation illustarted by Drosophila Shaker (PDBid 7SIP)**. Column 2:** Conducting pore conformation of Kv1.3 illustrated by structure of Kv1.3 in complex with fab-ShK (PDBid 7SSV). **Column 3:** C-type inactive channl conformation illustrated by Shaker carrying the W434F mutation. **Column 4 and 5:** cryoEM structures of Kv1.3 in complex with either **4** or **7**. **Row A:** Side view of selectivity filter. Potassium ions are shown as spheres while selectivity filter residues and compounds **4** and **7** are shown as sticks. **Row B:** Key hydrogen bond stabilizing the active and conducting pore conformation is broken for Kv1.3 in complex with either **4** or **7**. Note for the Shaker W434F, residue 434 is mutated to Phe thus stabilizing the inactive conformation. **Row C:** Hydrogen bonding between Kv1.3 Tyr ^{447} and Thr^{441} is broken upon **4** or **7** binding. Note that Tyr447 adopts two conformations in structures of Kv1.3 bound to **4** or **7**. Tyr447 rotamer 1 engange in new hydrogen bonding with Trp436 from adjecent protomer while rotamer 2 adopt conformation like the C-type inactive Shaker W434F.

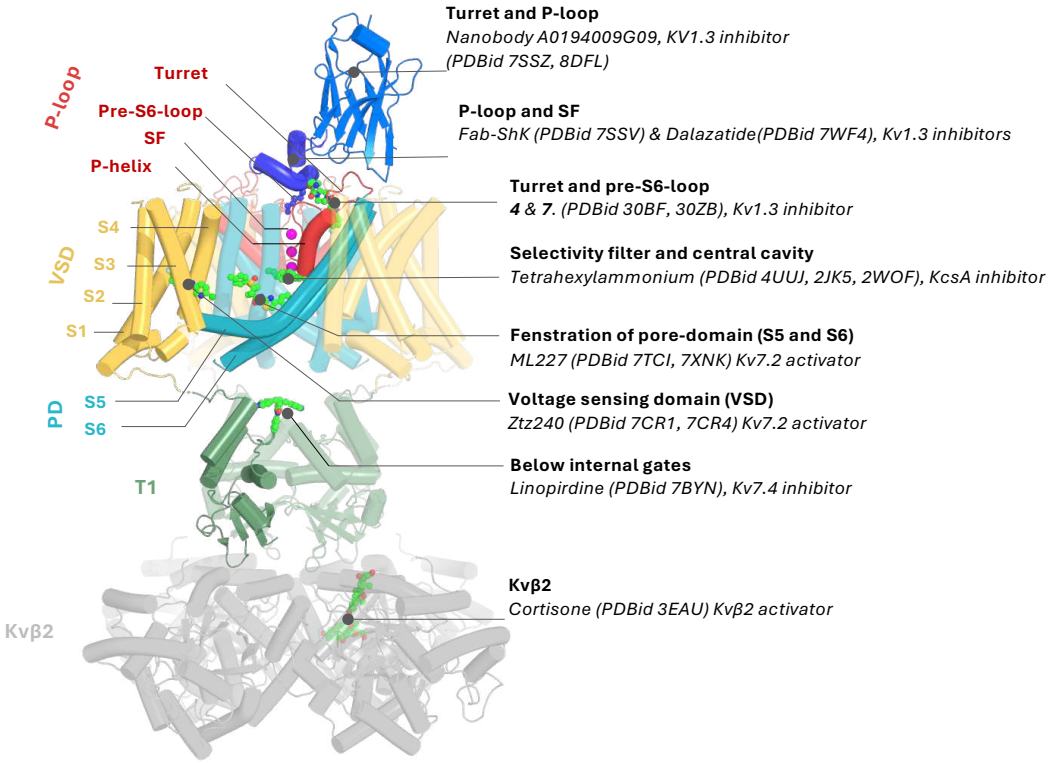


Figure 8. Binding sites of example Kv and KcsA modulators with experimental structural data.

Supplementary Files

This is a list of supplementary files associated with this preprint. Click to download.

- Suppmaterialsandmethods.docx
- Table1.pdf
- Table2.pdf
- SuppTable1.pdf
- wwPDBEMValidationreport30BFEMD57536.pdf
- Additionalinformation.docx